Simulation and experimental characterization of the point spread function, pixel saturation, and blooming of a mercury cadmium telluride focal plane array

Grant Soehnel* and Anthony Tanbakuchi

Sandia National Laboratories, 1515 Eubank SE, Albuquerque, New Mexico 87123, USA

*Corresponding author: gsoehne@sandia.gov

Received 28 August 2012; revised 17 October 2012; accepted 18 October 2012;
posted 19 October 2012 (Doc. ID 175117); published 19 November 2012

A custom IR spot scanning experiment was constructed to project subpixel spots on a mercury cadmium telluride focal plane array (FPA). The hardware consists of an FPA in a liquid nitrogen cooled Dewar, high precision motorized stages, a custom aspheric lens, and a 1.55 and 3.39 μm laser source. By controlling the position and intensity of the spot, characterizations of cross talk, saturation, blooming, and (indirectly) the minority carrier lifetime were performed. In addition, a Monte–Carlo-based charge diffusion model was developed to validate experimental data and make predictions. Results show very good agreement between the model and experimental data. Parameters such as wavelength, reverse bias, and operating temperature were found to have little effect on pixel crosstalk in the absorber layer of the detector. Saturation characterizations show that these FPAs, which do not have antiblooming circuitry, exhibit an increase in cross talk due to blooming at ~39% beyond the flux required for analog saturation.

OCIS codes: 040.1240, 040.3060, 120.0120.

1. Introduction

Focal plane arrays (FPAs) introduce blurring into an optical system due to cross talk in which a signal incident on a pixel is read out by another pixel. The primary mechanism that produces cross talk is charge diffusion in the absorber layer. In order to characterize these effects, a spot scanning experiment was constructed to approximate a point source of light on a mercury cadmium telluride (MCT) IR FPA at 1.55 and 3.39 μm. The position of the spot is controlled by motorized translation stages. This experiment allows for direct measurement of the point spread function (PSF) of the detector [1,2], which is a pixel's response to point illumination as a function of position in the plane of the detector. The PSF depends on the physics of charge diffusion in conjunction with the pixel geometry and location of the illumination.

In order to validate spot scanning data and obtain a predictive tool, a charge diffusion simulation was developed. A Monte Carlo-style approach was utilized [3] in which photons are absorbed and treated by the simulation one at a time. At the point of absorption, the resulting minority carrier is tracked through a random walk in the absorber layer until it either recombines or is collected. This approach is time consuming due to the large number of photons that must be simulated, but it is desirable due to the ease with which design parameters and geometry can be altered in three-dimensional space.

1559-128X/12/337987-07$15.00/0

The remainder of this paper is organized as follows. In Section 2 details about the spot scanning experiment will be provided. In Section 3 the charge diffusion model will be explained. Results are presented in Section 4, including nominal PSFs in Subsection 4.A and saturation experiments and modeling in Subsection 4.B. Finally, conclusion will be given in Section 5.

2. Spot Scanning Experiment

A diagram containing the primary components of the spot scanning experiment is illustrated in Fig. 1. A laser is coupled to a single mode fiber, and the illuminated fiber core is reimaged to form the spot on the FPA surface. The primary laser used is a fiber coupled laser at 1.55 μm. The laser is normally used in cw mode, but the option exists to modulate the laser with an external voltage source. The system is also designed to use a 3.39 μm He–Ne laser, which is then coupled in free space to a fiber. The lens is a custom asphere, designed to balance aberrations caused by the window and filter in the Dewar (not shown) between the lens and FPA from 1.55 to 3.39 μm. The lens, fiber, and a fold mirror are all mounted on a three-dimensional translating platform to move the spot, while the FPA remains stationary.

The alignment of the system is made difficult, because the wavelength is invisible and the lens is opaque to visible light. It is made easier, however, due to there being only one lens to align with the fiber face. Two alignment telescopes (theodolites) were used that project a target with a visible laser. The two were aligned to each other centered through the empty fiber mount without the lens present, and then the lens was added and centered/tilted to align with both telescopes. It was also found that a more simple method of aligning the fiber mount and lens with a visible laser is adequate as well. Mirrors can be inserted and removed from the fiber and lens mount to align the tilt of both elements/mounts, and the backreflection off the lens itself without the mirrors can be used to center the lens. This method requires that mirrors can be added to the fiber and lens mounts with certainty that the tilt of the mirrors match the tilt of the fiber and lens.

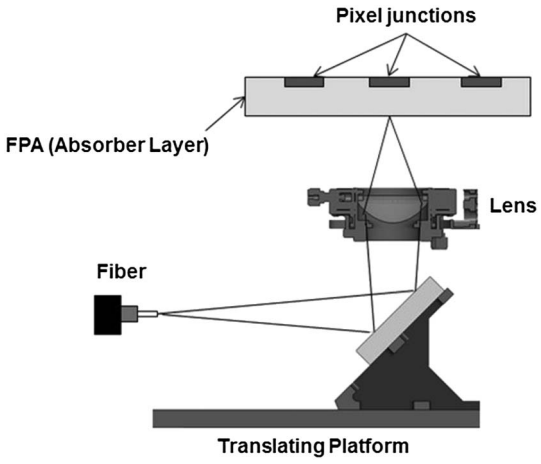

Fig. 1. Diagram of spot scanning experiment.

The FPA is custom designed and has a backside-illuminated MCT absorbing layer with p-type implants forming junctions that define each pixel. Photogenerated carriers diffuse in the absorber layer until they either recombine or are collected at a junction. Carriers that are generated in one pixel and diffuse to another before they are collected cause cross talk. As indicated in Fig. 1, the absorber layer for this FPA does not contain any etched divisions between pixels. Etching into the absorber layer to separate pixels is a common practice and does reduce cross talk, though the extra surface area increases recombination and lowers the quantum efficiency.

The spot is focused and centered on a pixel by adjusting all three motorized stages to maximize the signal output from a pixel while also keeping the responses of the surrounding pixels symmetrical. An automated routine has been created that iterates between a centering adjustment and a focus adjustment to position the spot and begin a scan. A two-dimensional scan with a 2 μm step size is then performed to measure the detector PSF. The PSF is the relative response of a single pixel to flux falling on points in the two-dimensional surface centered on the pixel. The PSF measured directly by the spot scanning experiment, $\mathrm{PSF}_{\mathrm{measured}}$, differs from the actual PSF, $\mathrm{PSF}_{\mathrm{detector}}$, because the spot used for the measurement is not infinitely small. The relation of the two is [2]

$$\mathrm{PSF}_{\mathrm{measured}} = \mathrm{PSF}_{\mathrm{optics}} * \mathrm{PSF}_{\mathrm{detector}}, \tag{1}$$

where $(*)$ indicates a convolution and $\mathrm{PSF}_{\mathrm{optics}}$ is the relative flux profile of the spot itself. A deconvolution using the MATLAB function "deconvlucy" of the spot profile was performed on all the data to extract the detector PSF from the measured PSF. The conditions for the deconvolution are favorable in that the spot profile is quite small when compared to the width of the PSF. The spot profile was modeled based on the optical design and verified with a knife edge profile measurement. The spot size in relation to the pixel size is shown in Fig. 2. The modulation transfer function (MTF) is also computed by performing a Fourier transform on the PSF [4]. The relation of the detector MTF to the measured MTF is [2]

$$\mathrm{MTF}_{\mathrm{measured}} = \mathrm{MTF}_{\mathrm{optics}} \cdot \mathrm{MTF}_{\mathrm{detector}}. \tag{2}$$

Performing a Fourier transform on $\mathrm{PSF}_{\mathrm{measured}}$ and $\mathrm{PSF}_{\mathrm{optics}}$ to get $\mathrm{MTF}_{\mathrm{measured}}$ and $\mathrm{MTF}_{\mathrm{optics}}$ allows for a division according to Eq. (2) to obtain $\mathrm{MTF}_{\mathrm{detector}}$. This is the preferred method, because it avoids the deconvolution step.

3. Charge Diffusion Model

In order to validate data produced by the spot scanning experiment, a charge diffusion model was

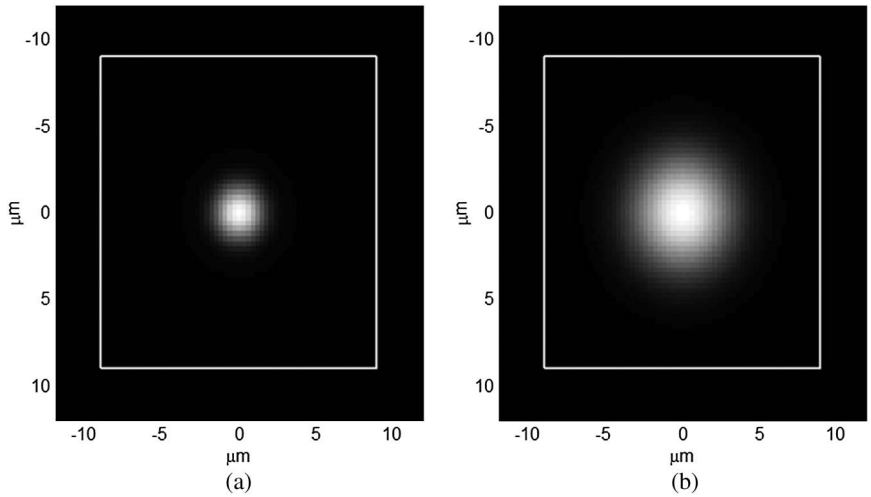

Fig. 2. Spot size in comparison to pixel size (white box) at the two wavelengths of (a) 1.55 μm and (b) 3.39 μm.

developed. The approach used is a Monte–Carlo simulation in which minority carriers are generated and collected one at a time. Figure 3 illustrates the steps of the simulation for each carrier. A carrier is generated [Fig. 3(a)] at a random depth according to the absorption coefficient α modeled by the following equations [5]:

$$E_g = -0.295 + 1.87x - 0.28x^2 + 0.35x^4 + T(6 - 14x + 3x^2) \cdot 10^{-4}, \quad (3)$$

$$\alpha_g = -65 + 1.88T + (8694 - 10.31T)x, \quad (4)$$

$$\beta = -1 + 0.083T + (21 - 0.13T)x, \quad (5)$$

$$\alpha = \alpha_g \exp\left(\sqrt{\beta(E - E_g)}\right), \quad (6)$$

where x is the cadmium concentration, T is the temperature (K), E is the photon energy, and E_g is the bandgap (eV). The lateral position can be at a single point or can follow a user-defined flux distribution. In the latter case, each lateral position of a photogenerated carrier is randomly generated according to the flux distribution. In practice, a common choice for the flux distribution is the optical spot profile. From the point of generation, carriers are tracked through a random walk [Fig. 3(b)] according to their velocity v and the mean free time between collisions τ defined by [6]

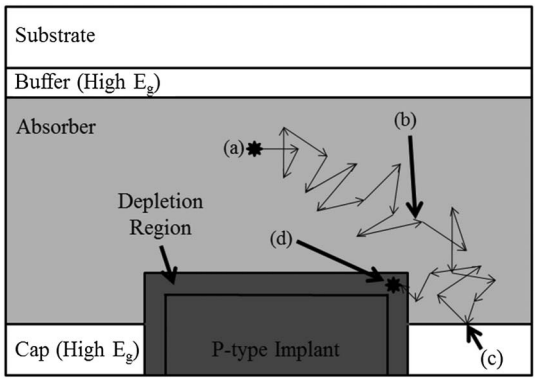

Fig. 3. Illustration of a single pixel and the charge diffusion simulation approach. (a) Carrier generation, (b) carrier diffusion (random walk), (c) reflection at the cap or buffer layer, and (d) collection.

$$v = \left(\frac{3kT}{m_e}\right)^{\frac{1}{2}}, \quad (7)$$

$$\tau = \mu \cdot \frac{m_e}{q}, \quad (8)$$

where v is the thermal velocity, μ is the mobility, m_e is the effective mass, q is the charge of an electron ($1.6 * 10^{-19}$), and k is the Boltzmann constant ($1.38065 * 10^{-23}$). Each collision results in a random change in direction. For this detector design, surface recombination at the boundaries of the absorber layer is very low due to a high bandgap cap and buffer layer. If a carrier encounters one of these boundaries, it is specularly reflected at the boundary [Fig. 3(c)]. When a carrier enters the depletion region of a pixel junction, it is collected and the simulation ends for that carrier [Fig. 3(d)]. The depletion region contains the electric field due to a built-in voltage as well as an applied bias, and the width W_D is computed by [6]

$$W_D = \left(\frac{12\varepsilon_s(V_{\text{bi}} + V)}{q \cdot a}\right)^{\frac{1}{3}}, \quad (9)$$

where V_{bi} is the built in voltage, V is the applied bias, a is the impurity gradient of the junction (assumed to be linearly graded), and ε_s is the permittivity. Finally, each carrier has a total lifetime (before recombination) randomly assigned to it according

to an exponential distribution and the mean total lifetime. The mean total lifetime was provided in material properties for this device, but impurities that cause nonradiative recombination add a degree of uncertainty. It was found that experimental data presented in Subsection 4.B, studying saturation and blooming, can be used to estimate and adjust the mean total lifetime.

4. Results

The spot scanner was used to measure the nominal unsaturated PSF as a function of wavelength, operating temperature, reverse bias, and spatial location on the FPA. In order to view and compare PSFs, the radial average was computed and then mirrored to imitate a cross section. There were slight asymmetries in the two dimensional PSFs due to the pixels being arranged on a square grid spacing. Simulated results were compared to experimental data. Intensity sweeps were then performed to measure pixel responses up to and far beyond the saturation level of a single pixel. The onset of blooming was clearly identified with these data, and the simulation was updated to incorporate saturation.

A. Nominal Point Spread Functions

Spot scanning results under normal operating parameters are presented in Fig. 4. The dataset was produced by scanning 32 pixels that were clustered in four groupings of 8 pixels. Each grouping contained pixels all from a localized region of the FPA. Plots of all 32 pixel PSF [Fig. 4(a)] and MTF [Fig. 4(b)] curves show that there is little variation. The mean PSF [Fig. 4(c)] and MTF [Fig. 4(d)] curve for each grouping was also computed. These four curves show that the PSF does exhibit small spatial variations within the FPA, which could be caused by variations in the absorber layer thickness.

Figure 5 presents PSF and MTF curves as the reverse bias is varied. The same 32 pixels were scanned at each of four different reverse bias voltages. Figures 5(a) and 5(b) show the mean PSF and MTF at each of the voltages, and Figs. 5(c) and 5(d) present a cropped plot centered at 10% of the maximum value. The 10% level is chosen because this is the region with the largest variations in the PSF curves. Figures 5(c) and 5(d) also contain simulation results (dashed curves). As the reverse bias increases, the depletion region width increases and carriers are collected more readily before diffusing to another pixel. The difference is small, but averaging 32 pixels did produce a clear distinction that the PSF gets tighter with increasing reverse bias. The simulation was also able to produce this small but distinct result very accurately.

Figure 6 presents PSF and MTF curves for a dataset in which the operating temperature was varied. 32 pixels were scanned at each operating temperature, and the curves of Fig. 5 are each an average for all 32 pixels. Similar to the reverse bias dataset,

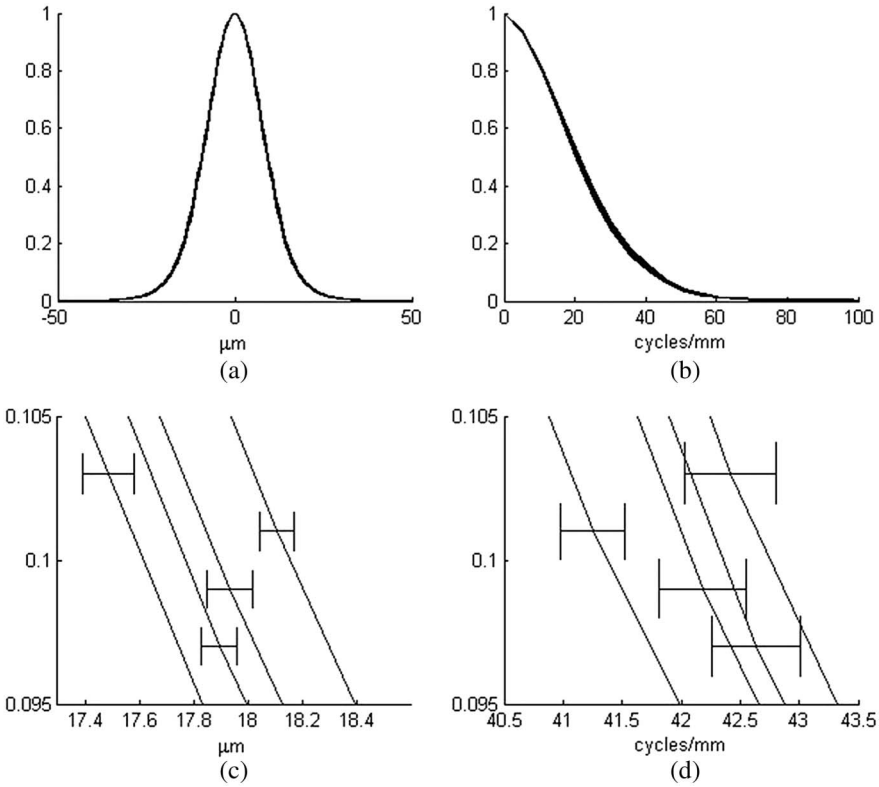

Fig. 4. PSF and MTF curves under normal operating parameters for 32 pixels. (a) PSFs, (b) MTFs, (c) mean PSF curves for four groupings of 8 pixels coming from localized regions of the FPA with ±1 standard deviation widths shown (plots are cropped to show curves near 10% of the maximum value), and (d) mean MTF curves for the same four groupings.

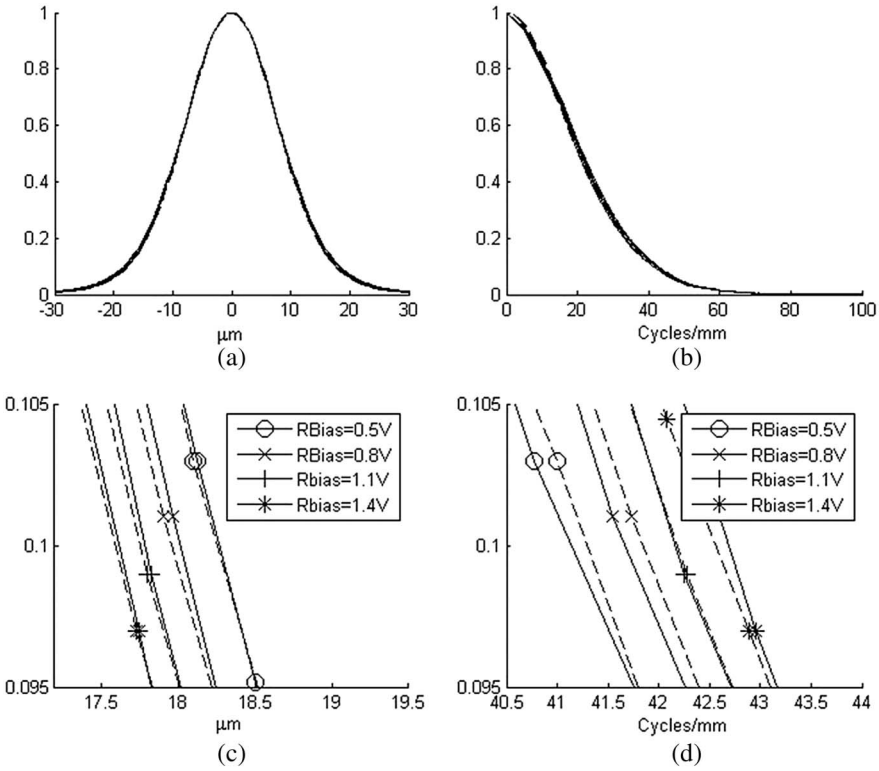

Fig. 5. PSF and MTF curves as reverse bias is varied. (a) Mean PSF curve at four biases, (b) mean MTF curve at four biases, (c) data (solid curves) and model (dashed curves) PSF curves zoomed in at ~10% of the maximum value, and (d) MTF curves.

this dataset did not show any significant changes in the PSF. The slight trend of a tighter PSF with decreasing temperature predicted by the simulation was not very clear in the data. It was difficult to obtain good data at such high operating temperatures, due to high dark currents limiting the dynamic

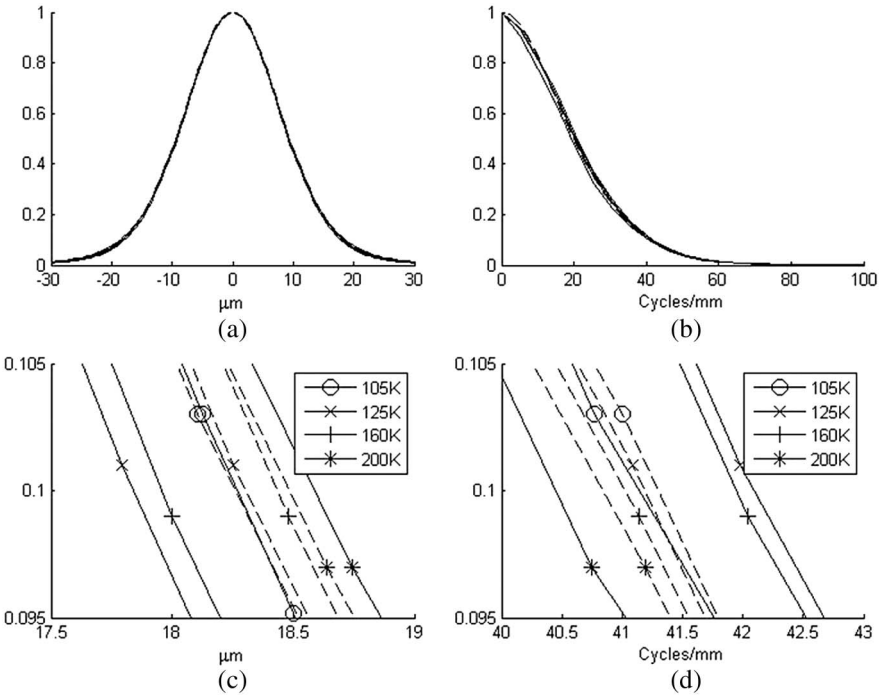

Fig. 6. PSF and MTF curves as operating temperature is varied. (a) Mean PSF curve at four temperatures, (b) mean MTF curve at four temperatures, (c) data (solid curves) and model (dashed curves) PSF curves zoomed in around 10% of the maximum value, and (d) MTF curves.

range and higher noise levels. The data do generally prove that charge diffusion and cross talk are not significantly impacted by temperature. Other data collected using both 1.55 and 3.39 μm illumination concluded that the incident wavelength has little effect on charge diffusion and cross talk.

B. Saturation and Blooming

To characterize pixel saturation and blooming, intensity sweeps were performed with the spot centered on a pixel. The 1.55 μm laser has the option to adjust or even modulate the intensity accurately with a voltage input. Initially the center pixel and the 8 pixels in the surrounding 3 × 3 grid were observed. The responses of the 4 pixels sharing a side were averaged together, and the same was done for the 4 pixels sharing a corner. The resulting curves of response versus power for a single intensity sweep are presented in Fig. 7. Abrupt changes in the response slope occur when excess saturating charge in the amplifier of the pixel unit cell erodes the bias on a pixel to the point where it becomes forward biased. When this happens, the pixel no longer collects minority carriers, and charge diffusion brings carriers generated in the now "dead" pixel to surrounding pixels. This process in which pixels become forward biased and stop collecting carriers due to saturation is known as blooming. The onset of blooming for a given pixel is defined as the point at which it no longer accepts carriers. It is clear that side and corner pixels show an uptick in response corresponding to the onset of blooming in the center pixel. Later, the corner pixels show an uptick in response when the side pixels begin to bloom. The onset of blooming was computed by fitting lines to the linear segments of the side pixels before and after the center pixel blooms and calculating the intersection. This was done for intensity sweeps on 32 different pixels, and the average result was that the onset of blooming is ~39% beyond the flux required to saturate a pixel. The onset happens fast enough for a bright saturating point source to bloom into pixels far beyond the pixel at which it is located. This is undesirable, because it will lead to a loss of valid data in the region suffering from blooming.

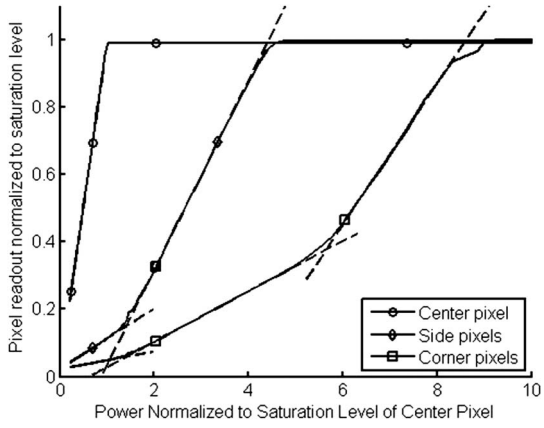

Fig. 7. Response versus power curves for a 3 × 3 grouping of pixels with illumination incident on only the center pixel.

The onset of blooming was incorporated into the simulation by halting the accumulation of signal at a defined saturation level, then closing off the depletion region of a pixel at 39% beyond the point of saturation. Simulations were performed using the actual spot profile in order to match the saturated data taken with the intensity sweeps. One additional adjustment was made to the carrier lifetime in order to calibrate the model to the data. Under extreme saturation, minority carriers must travel long distances before reaching a still functioning pixel. When a significant number start recombining before reaching the edge of the saturated spot, it serves to slow down the rate at which the spot can expand with increasing illumination. This afforded an opportunity to adjust the total minority carrier lifetime to match the outward rate of blooming in the simulation to the lab data. The best fit total lifetime was found to be ~0.78 μs, and resulting data—simulation comparisons are shown in Fig. 8. The data match the simulation very closely in terms of spot size, but the edges of the spot exhibit more blurring in the data, particularly at the 1000× saturation level. This could be due to the actual spot profile containing very low level flux far from the center that is not modeled. The modeled spot profile exists in a 9 × 9 pixel grid. The flux reduces to near zero by the edges of this grid. In reality, stray light and double reflections could be producing small but nonzero flux extending far from the center that was not modeled and is very difficult to measure. This is normally not an issue for spot measurements, but when the intensity is increased to 1000× saturation, it could be blurring the edge

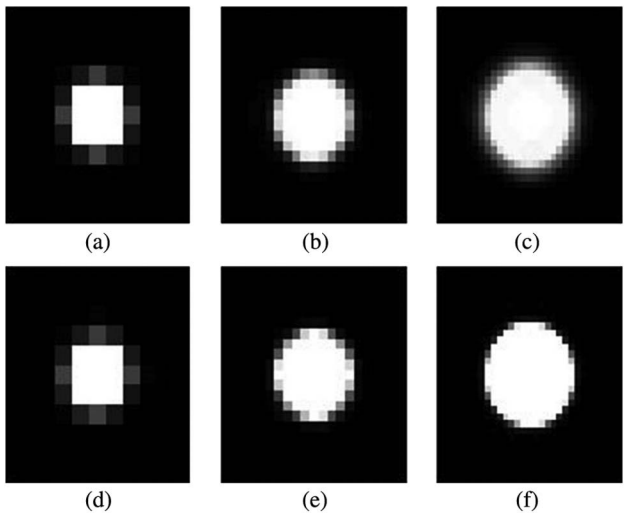

Fig. 8. Frames obtained from data and simulation with illumination incident on a single pixel. (a) Data at 10× the saturation level of the illuminated pixel (11 × 11 pixels shown), (b) data at 100× saturation (21 × 21 pixels shown), (c) data at 1000× saturation (31 × 31 pixels shown), (d) simulation at 10× saturation (11 × 11 pixels shown), (e) simulation at 100× saturation (21 × 21 pixels shown), and (f) simulation at 1000× saturation (31 × 31 pixels shown).

of the outward blooming spot. A blooming spot with no flux near the edges would expand outward with a sharp edge, but a broad flux near that edge could blur it.

5. Conclusions

This work has resulted in a broad understanding of charge diffusion and blooming in MCT FPAs. The charge diffusion simulation proved to match lab data very well in a variety of experiments. It was found that there is little variation in the nominal PSF for a given detector design. The spatial location, temperature, reverse bias, and wavelength all have little effect on the PSF. Fundamental design parameters such as absorber layer thickness and pixel pitch are more likely to affect the PSF, and these parameters could be studied using the simulation. In addition, the onset of blooming and the minority carrier lifetime were determined through data collection and simulation. This in turn allowed for very accurate modeling of severely saturated spots on the FPA. This capability could be used to estimate the energy content of a saturated region of pixels.

Sandia National Laboratories is a multiprogram laboratory operated by Sandia Corporation, a Lockheed-Martin Company, for the United States Department of Energy under Contract No. DE-AC04-94AL85000. This work was supported by Sandia's Laboratory Directed Research and Development Program.

References

1. J. D. Bray, L. Schumann, and T. Lomheim, "Front-side illuminated CMOS spectral pixel response and modulation transfer function characterization: impact of pixel layout details and pixel depletion volume," Proc. SPIE **7405**, 74050Q (2009).
2. J. Bray, K. Gaab, B. Lambert, and T. Lomheim, "Improvements to spectral spot-scanning technique for accurate and efficient data acquisition," Proc. SPIE **7405**, 74050L (2009).
3. J. Lavine, W. Chang, C. Anagnostopoulos, B. Burkey, and E. Nelson, "Monte Carlo simulation of the photoelectron crosstalk in silicon imaging devices," IEEE Trans. Electron Devices **32**, 2087–2091 (1985).
4. J. Goodman, *Introduction to Fourier Optics* (Roberts, 2005).
5. P. Capper and J. Garland, *Mercury Cadmium Telluride, Growth, Properties, and Applications* (Wiley, 2011).
6. S. Sze and K. Ng, *Physics of Semiconductor Devices* (Wiley, 2007).